Hadley Circulation Response to Orbital Precession. Part II: Subtropical Continent

TIMOTHY M. MERLIS

Princeton University, and Geophysical Fluid Dynamics Laboratory, Princeton, New Jersey

TAPIO SCHNEIDER AND SIMONA BORDONI

California Institute of Technology, Pasadena, California

IAN EISENMAN

Scripps Institution of Oceanography, University of California, San Diego, La Jolla, California

ABSTRACT

The response of the monsoonal and annual-mean Hadley circulation to orbital precession is examined in an idealized atmospheric general circulation model with a simplified representation of land surface processes in subtropical latitudes. When perihelion occurs in the summer of a hemisphere with a subtropical continent, changes in the top-of-atmosphere energy balance, together with a poleward shift of the monsoonal circulation boundary, lead to a strengthening of the monsoonal circulation. Spatial variations in surface heat capacity determine whether radiative perturbations are balanced by energy storage or by atmospheric energy fluxes. Although orbital precession does not affect annual-mean insolation, the annual-mean Hadley circulation does respond to orbital precession because its sensitivity to radiative changes varies over the course of the year: the monsoonal circulation in summer is near the angular momentum-conserving limit and responds directly to radiative changes; whereas in winter, the circulation is affected by the momentum fluxes of extratropical eddies and is less sensitive to radiative changes.

1. Introduction

The effect of orbital precession on the mean meridional circulation of the tropical atmosphere is examined in an idealized atmospheric general circulation model (GCM) that includes a representation of land surfaces. Building on the results of a companion paper that examines aquaplanet simulations (Merlis et al. 2013a, hereafter Part I), we investigate how land surfaces modify the response of the atmospheric circulation to orbital precession. Our goal is to understand simulations that bridge the gap between aquaplanet simulations (Part I) and comprehensive GCM simulations (e.g., Kutzbach 1981; Clement et al. 2004). The idealized GCM simulations that we present are useful in this respect because they feature poleward shifts in convergence

zones and strengthened divergent circulations near continental boundaries in response to precession-forced insolation increases, as has been found in comprehensive GCM simulations (Braconnot et al. 2007; Clement et al. 2004). The simulations also allow us to connect with the literature on monsoonal circulations that focuses on the effect of the reduced surface heat capacity of land and its role in generating land–sea breeze circulations.

How might land surfaces affect the response of the atmospheric circulation to orbital precession? It is conceptually useful to separate ideas about the atmospheric circulation into those based on surface considerations and those based on top-of-atmosphere energy balance considerations. For example, the common interpretation of monsoons as land–sea breeze circulations emphasizes the surface temperature gradient, which can affect the surface winds by modifying pressure or geopotential gradients that enter the horizontal momentum equation (e.g., Lindzen and Nigam 1987). In contrast, angular momentum-conserving Hadley circulation theories estimate the strength of the Hadley circulation, in

Corresponding author address: Timothy M. Merlis, Princeton University, and Geophysical Fluid Dynamics Laboratory, Jadwin Hall, Princeton, NJ 08544.
E-mail: tmerlis@princeton.edu

an energetic sense, from the top-of-atmosphere energy balance (Held and Hou 1980).

We found in Part I that the response of the monsoonal Hadley circulation to orbital precession can be understood on the basis of top-of-atmosphere energetics. This is consistent with Kang and Held (2012), who advocate for the primacy of the energetic perspective over surface perspectives (e.g., Lindzen and Nigam 1987) in understanding the precipitation response to cross-equatorial ocean energy fluxes. However, we also showed in Part I that the surface enthalpy distribution is important in determining the gross moist stability—the energetic stratification that determines the relationship between energy and mass fluxes.

Following previous work, we interpret monsoons as regional manifestations of the seasonal migration of the convergence zones of large-scale circulations such as the Hadley circulation (Chou et al. 2001; Chao and Chen 2001; Gadgil 2003; Privé and Plumb 2007; Bordoni and Schneider 2008). The ascending branch of the cross-equatorial Hadley circulation, which we refer to as the monsoonal Hadley circulation, is typically close to the angular momentum-conserving limit and so can respond directly to energetic changes. However, surface thermodynamics can play a role in this limit. First, as in Part I, thermodynamic changes at the surface can modify the gross moist stability. Second, as in Privé and Plumb (2007), the surface moist static energy distribution can determine the location of the ascending branch of monsoonal Hadley circulations; this argument is reviewed in the appendix. Third, variations in the surface heat capacity lead to regional and time-dependent differences in the enthalpy fluxes from the surface to the atmosphere (e.g., Neelin 2007).

As a lower boundary condition for the atmosphere, land regions differ from ocean regions in several ways: they have lower surface heat capacity, a limited evaporation reservoir, different surface albedo and orography, and they lack fluid energy transports. Some surface processes will modify the mean climate but will not affect the response to radiative perturbations. For example, introducing hemispheric asymmetry in the prescribed ocean energy flux divergence in the atmospheric GCM simulations presented here changes the mean climate but has little effect on the precession-forced changes. We are interested in examining surface processes that mediate the climate response to orbital precession, that is, those that interact with the radiative changes. This guides our choice of simulations presented. We focus on simulations with regions of reduced surface heat capacity with or without a representation of land surface hydrology.

We examine how the Hadley circulation responds to orbital precession in simulations with idealized subtropical continents. We find that the mass flux of monsoonal Hadley circulations can increase when summers receive more insolation, and this seasonal change can affect the annual-mean Hadley circulation. The summer season changes in the Hadley circulation can be understood by examining the role of the inhomogeneous surface heat capacity on atmospheric energetics and the role of the surface moist static energy distribution in determining the location of the ascending branch of monsoonal circulations. The dynamics responsible for generating the annual-mean changes in the Hadley circulation are governed by a mechanism that appears not to have been documented before. The insolation changes affect the Hadley circulation in the summer season more than in the winter season because of the seasonality of the angular momentum balance regime. The monsoonal Hadley circulation in the summer hemisphere is close to the angular momentum-conserving limit, so it responds directly to thermodynamic and energetic changes. In the winter hemisphere, the angular momentum balance of the descending branch of the monsoonal Hadley circulation is affected by the energy-containing extratropical eddies in addition to the circulation's nonlinear momentum advection. So, the descending branch of the circulation is not free to respond directly to energetic changes, such as those due to top-of-atmosphere insolation variations.

2. Idealized GCM

The simulations presented here use an idealized GCM with the same atmospheric component as that described in Part I. The default surface heat capacity is that of 20 m of water (rather than 5 m in Part I); this is closer to estimates for Earth's oceans and provides a clear contrast relative to the land region. We present averages over the last 20 years of a simulation following a 10-yr spinup period, as in Part I. The substantial changes to the GCM are those associated with including representations of land surface processes in the lower boundary condition, as described in what follows.

a. Continent geometry

The continent geometry used in the simulations is a zonally symmetric, Northern Hemisphere subtropical continent extending from 10° to 30°N (Fig. 1). This range of latitudes is chosen so that the continent is in latitudes characteristic of Northern Hemisphere tropical landmasses such as the African Sahel and southern India. It is also a region of annual-mean water vapor flux divergence, and Earth's deserts are located in these subtropical latitudes. Previous work suggests that the placement of the southern boundary of continents can
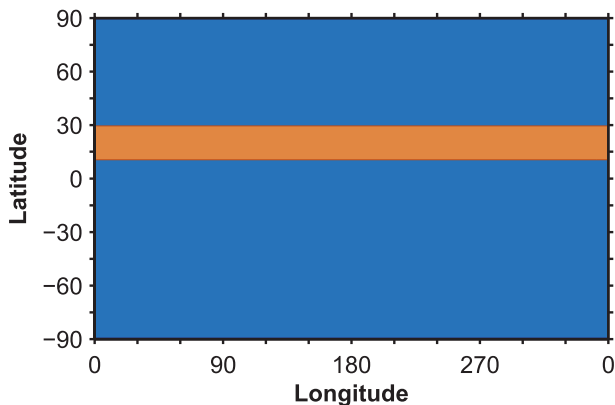
FIG. 1. Latitude–longitude view of the Northern Hemisphere subtropical continent boundaries, with orange indicating land and blue indicating ocean.

have a substantial impact on precipitation (Dirmeyer 1998), but we have not varied this aspect of the surface boundary condition.

b. Land model description

Land and ocean differ in several ways. The idealized land model that we use accounts for the differences in heat capacity, the limited evaporation reservoir, and lack of ocean energy flux divergence over land, while it neglects orography and albedo differences.

The evolution equation for the mixed layer surface temperature T_s is

$$\rho_o c_{po} d \frac{\partial T_s}{\partial t} = S_{\text{surf}} - L_{\text{surf}} - LE - H - \mathbf{V} \cdot \mathbf{F}_o, \quad (1)$$

with ocean density ρ_o, ocean heat capacity c_{po}, ocean mixed layer depth d, net shortwave surface radiation S_{surf}, net longwave surface radiation L_{surf}, latent enthalpy flux LE, sensible enthalpy flux H, and ocean energy flux divergence $\mathbf{V} \cdot \mathbf{F}_o$. The land model consists of modifying $\rho_o c_{po} d$ to account for the inhomogeneous surface heat capacity, modifying LE to account for the limited evaporation reservoir of land surfaces, and setting $\mathbf{V} \cdot \mathbf{F}_o = 0$ to account for the lack of ocean energy flux divergence in land regions.

The land–sea contrast in heat capacity can be modeled by replacing the constant mixed layer depth d in (1) with a mixed layer depth $d(\lambda, \phi)$ that depends on longitude λ and latitude ϕ. In the model, we express the lower heat capacity of land through changes in the mixed layer depth d, while retaining ocean values for ρ_o and c_{po}. The product of typical values for soil density and specific heat are almost an order of magnitude smaller than those of water: $(\rho c_p)_{\text{land}} \approx 0.15$–$0.3 \times \rho_o c_{po}$ (e.g., Pierrehumbert 2010). Temperature perturbations

diffuse to a depth that depends on material conductivity κ and forcing frequency ω: $d \sim (\kappa \rho^{-1} c_p^{-1} \omega^{-1})^{1/2}$. For typical soil conductivities ($\kappa \approx 0.1$–0.3 W m^{-2} K^{-1}), this depth is ≈ 1 m for the seasonal cycle (e.g., Pierrehumbert 2010). For land regions, we therefore set the mixed layer depth $d = 0.2$ m. One relevant nondimensional parameter is the ratio of the land heat capacity to the atmospheric heat capacity (≈ 2 m of water); it is likely that the simulation results are not too sensitive to small variations in this parameter when it is sufficiently smaller than one. Also, with these parameters the response time of the land surface is short compared with the seasonal cycle.

To model the limited evaporation reservoir over land surfaces, a "bucket depth" variable b is added to the GCM. The bucket depth changes in response to net precipitation, $P - E$:

$$\frac{\partial b}{\partial t} = P - E.$$

The standard bulk aerodynamic formula for evaporation,

$$E_0 = \rho c_d \|\mathbf{v}\| [q_s(T_s) - q]$$

with standard variable definitions, is modified to cap the evaporative flux of water when it would exceed the amount available at the surface:

$$E = \begin{cases} P, & \text{if} \quad P - E_0 < 0 \quad \text{and} \quad b = 0 \\ E_0, & \text{otherwise}. \end{cases}$$

Therefore, there is no net evaporation if there is no surface water available ($b = 0$).

The prescribed ocean energy flux divergence $\mathbf{V} \cdot \mathbf{F}_o$ (the Q flux) should be zero where there is land; that is, there are no fluid energy transports in the land surface. The basic climatological features of tropical precipitation, in particular the land–sea differences, depend on the spatial features of the ocean energy flux divergence (Chou et al. 2001). We have not considered how ocean circulation changes modify the climate response to orbital precession (cf. Kutzbach and Liu 1997).

In Part I, the divergence of the poleward ocean energy flux is represented by the function

$$\mathbf{V} \cdot \mathbf{F}_o(\phi) = Q_0 \frac{1}{\cos\phi} \left(1 - \frac{2\phi^2}{\phi_0^2}\right) \exp\left(-\frac{\phi^2}{\phi_0^2}\right), \quad (2)$$

which is inspired by reanalysis estimates (Bordoni 2007). Merlis and Schneider (2011) and Bordoni and Schneider (2008) neglected the $(\cos\phi)^{-1}$ factor, which results in a global-mean sink of energy of about 0.5 W m^{-2}. For

subtropical continents an alternative Q-flux formulation is required. The approach that we take is to use a different amplitude and width for the Q flux in the Northern Hemisphere (NH) and Southern Hemisphere (SH):

$$\mathbf{\nabla} \cdot \mathbf{F}_o(\phi) = \begin{cases} Q_{\mathrm{NH}} \dfrac{1}{\cos\phi} \left(1 - \dfrac{2\phi^2}{\phi_{\mathrm{NH}}^2}\right) \exp\left(-\dfrac{\phi^2}{\phi_{\mathrm{NH}}^2}\right), & \text{if} \quad \phi > 0 \\ Q_{\mathrm{SH}} \dfrac{1}{\cos\phi} \left(1 - \dfrac{2\phi^2}{\phi_{\mathrm{SH}}^2}\right) \exp\left(-\dfrac{\phi^2}{\phi_{\mathrm{SH}}^2}\right), & \text{if} \quad \phi < 0. \end{cases} \quad (3)$$

The width and amplitude parameter are reduced in the hemisphere with the subtropical continent: $Q_{\mathrm{NH}} = 10$ W m^{-2} and $\phi_{\mathrm{NH}} = 5°$ versus $Q_{\mathrm{SH}} = 50$ W m^{-2} and $\phi_{\mathrm{SH}} = 16°$. The Northern Hemisphere values are consistent with estimates of the ocean energy flux that assume the interior ocean stratification is adiabatic, the ocean mass transport is given by the Ekman transport (Klinger and Marotzke 2000), and the integral of the temperature flux is truncated at the latitude of the southern boundary of the continent; from this perspective, there is a weaker ocean energy transport when the continent is introduced because the subsurface equatorward flow is assumed to conserve the surface temperature at the continent boundary (here 10°) rather than that of the latitude where Ekman subduction would occur in the absence of land (~30°). The resulting Q flux is shown in the top panel of Fig. 2 (black solid line), along with the Q flux used in the aquaplanet simulations (black dashed line).

The ocean energy flux $\mathbf{F}_o$ is continuous across the equator (Fig. 2, bottom), but the meridional divergence of the flux $\mathbf{\nabla} \cdot \mathbf{F}_o$ is not. We have performed simulations in which the equatorial discontinuity in the Q flux is smoothed and the results are similar to those presented here.

c. Simulations

One can independently include aspects of the land model in the GCM. For example, if only the asymmetric Q flux is included, the mean climate changes (there is cooling and less precipitation in the Northern Hemisphere subtropics), but the climate response to orbital precession is similar to that of aquaplanet simulations with hemispherically symmetric Q flux (see Part I).

We focus on representations of land that modulate the precession-forced changes. In particular, we describe in detail simulations with reduced land heat capacity ("heat capacity simulations") and simulations with both surface hydrology and reduced land heat capacity ("surface hydrology simulations"). Both configurations include the hemispherically asymmetric Q flux.

As in Part I, we vary the phase of perihelion between the Southern Hemisphere summer solstice (referred to as "December perihelion"), which is similar to Earth's current perihelion phase, and the Northern Hemisphere summer solstice (referred to as "June perihelion") with eccentricity 0.05 and obliquity 23°. We use an eccentricity that is larger than that of Earth's current orbit so that the precession-forced insolation changes are larger. The resulting change in top-of-atmosphere insolation can be seen in Fig. 2 of Part I.

3. Surface climate and Hadley circulation

a. Heat capacity simulations

1) SURFACE CLIMATE

The seasonal cycle of surface temperature and precipitation for the heat capacity simulations is shown in Fig. 3. With the heat capacity of the continent in the Northern Hemisphere subtropics lower than the rest of the planet, the surface temperature in the continental region increases rapidly at the beginning of the Northern Hemisphere summer and decreases rapidly at the end (Figs. 3a,b). The relative warmth of the Southern Hemisphere subtropics is due to the larger Q flux in that hemisphere.

In the December perihelion simulation, the precipitation maximum migrates seasonally from 15°S to 8°N (Fig. 3c). The seasonal precipitation maximum does not extend as far poleward in the Northern Hemisphere as it does in the Southern Hemisphere as a result of the reduced Northern Hemisphere Q flux (Figs. 3c,d). However, it does extend farther poleward than in a simulation with a hemispherically asymmetric Q flux and no region of reduced heat capacity (not shown), suggesting that the reduced heat capacity does promote larger northward excursions of the precipitation maximum.

When the perihelion changes from December to June, the surface temperature over the continent increases with insolation (in May), whereas to the south of the continent there is some phase delay [changes are more prominent in August (Figs. 3a,b)]; this is the result of the inhomogeneous surface heat capacity. The June perihelion simulation has more precipitation near 15°N in Northern Hemisphere summer and less precipitation along the equator throughout the first half of the year
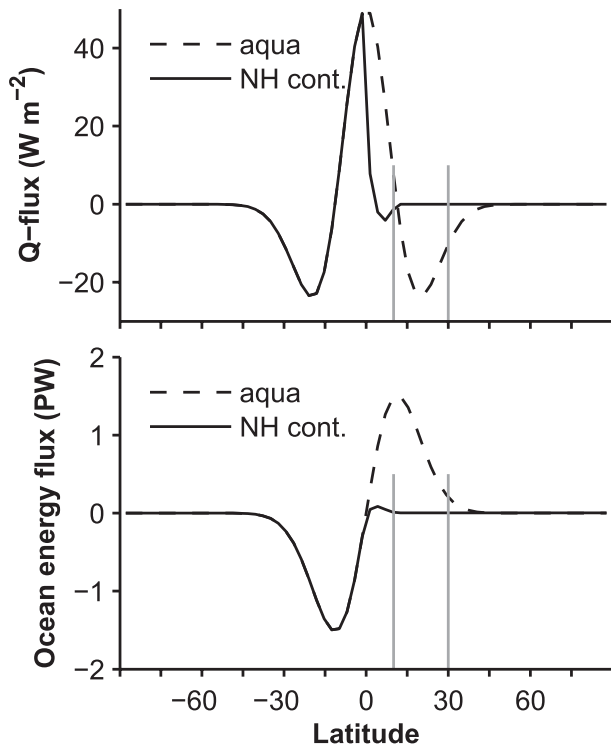
FIG. 2. (top) Ocean energy flux divergence, Q flux, and (bottom) ocean energy flux for Northern Hemisphere subtropical continent simulations (black solid line) and aquaplanet simulations of Part I (black dashed line). Vertical gray lines indicate the continent boundaries.

than the December perihelion simulation (Figs. 3c,d). Note that the Southern Hemisphere summer precipitation near 15°S increases even though there is less sunlight. The stronger Hadley circulation in that season (discussed in what follows) tends to increase precipitation by a greater amount than the changes in water vapor concentration, which tend to reduce precipitation there (the thermodynamic component of the water vapor flux changes is negative, while the dynamic component of the water vapor flux changes is positive and larger in magnitude; Merlis et al. 2013b).

2) HADLEY CIRCULATION

The annual-mean Hadley circulation of the December perihelion simulation is stronger in the Northern Hemisphere than in the Southern Hemisphere (Fig. 4, top). This is due to both asymmetry in the lower boundary condition—the atmosphere energy flux divergence must make up more of the top-of-atmosphere radiative imbalance in the Northern Hemisphere where the Q-flux is reduced—and precession forcing: the annual-mean Northern Hemisphere Hadley circulation is about 15% stronger than that of the Southern Hemisphere in a

corresponding December perihelion aquaplanet simulation with a hemispherically symmetric Q flux and a uniform surface heat capacity of 20 m of water. The Northern Hemisphere Hadley circulation remains stronger when the perihelion occurs in June (Fig. 4, middle), despite orbital forcing that, in isolation, leads to a stronger Southern Hemisphere Hadley circulation in this GCM (Part I). The annual-mean Hadley circulation weakens in both hemispheres when perihelion changes from December to June (Fig. 4, bottom). To understand why the Hadley circulation changes in this way, it is instructive to consider the seasonal circulations and their changes.

Figure 5 shows the Hadley circulation and its changes with perihelion averaged over two 6-month periods of the year: from June to November and December to May, where months are defined using fixed Julian days and the Northern Hemisphere autumnal equinox occurs on the same day for the different orbits. The months used in these averages are offset from the equinoxes as they better capture when the Hadley circulation's convergence zone changes hemispheres (Fig. 10); shifting the averaging period one month earlier or averaging from Northern Hemisphere summer solstice to winter solstice [i.e., averages that are based on angular position in the orbital plane; cf. Joussaume and Braconnot (1997)] gives similar results for Fig. 5 (and Fig. 8). Figure 5 shows that the annual-mean weakening of the Hadley circulation is actually the result of changes in the cross-equatorial, monsoonal Hadley circulations, which strengthen in both half years when perihelion changes from December to June. In the Northern Hemisphere cold season, the maximal monsoonal Hadley circulation mass flux in the lower troposphere ($\sigma = 0.67$) strengthens from 235×10^9 kg s^{-1} to 260×10^9 kg s^{-1} when the perihelion changes from December to June (left column of Fig. 5). In the Northern Hemisphere warm season, the monsoonal Hadley circulation shifts poleward and strengthens slightly (maximal lower troposphere mass flux increases from 238×10^9 kg s^{-1} to 245×10^9 kg s^{-1}) when perihelion changes from the December to June solstice (right column of Fig. 5). The Southern Hemisphere, which has uniform surface properties, exhibits a qualitatively similar response to precession changes as the aquaplanet simulations: Hadley circulation mass fluxes are weaker when the perihelion is in that season than when the aphelion is, though there are differences in the spatial structure and magnitude of the changes compared to aquaplanet simulations. The Northern Hemisphere, in contrast, exhibits the opposite sign response as in the aquaplanet simulations: Hadley circulation mass fluxes are stronger when perihelion is in that season. The warm season circulation changes are largest at the beginning of the
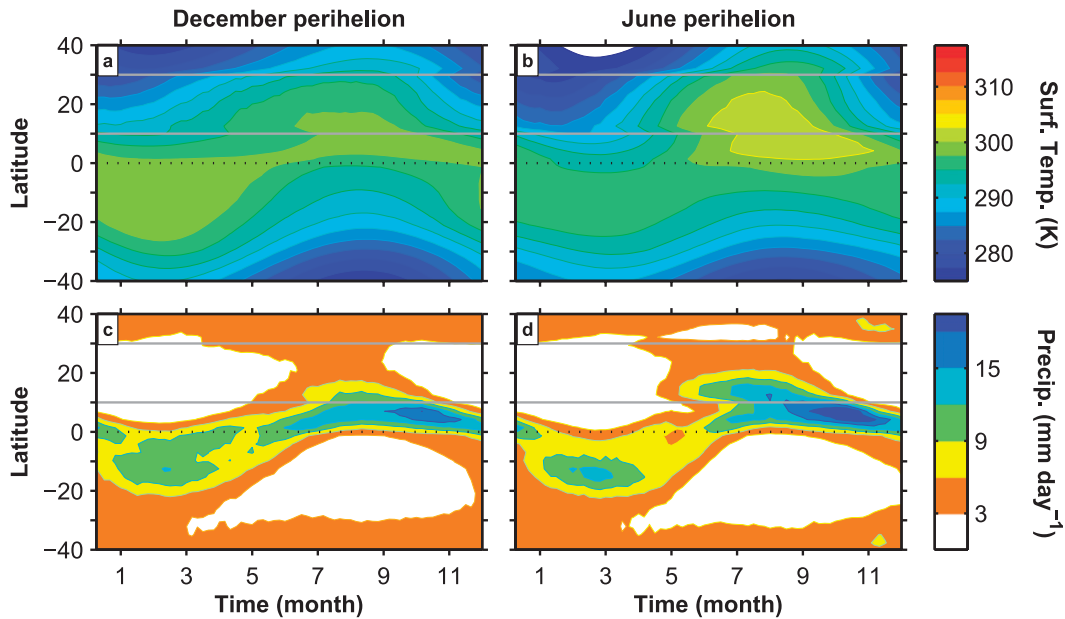
FIG. 3. (a),(b) Seasonal cycle of surface temperature and (c),(d) seasonal cycle of precipitation for heat capacity simulations with perihelion (a),(c) in December and (b),(d) in June. The contour interval is 2.5 K for surface temperature and 3 mm day^{-1} for precipitation, and the boundaries of the continent are shown in gray.

period when the convergence zone of the June perihelion simulation is in the Northern Hemisphere subtropics (Fig. 10). As the monsoonal Hadley circulation is near the angular momentum-conserving limit in the ascending branch (Fig. 11), it is instructive to consider the energetics of the atmospheric circulation (section 4).

b. Surface hydrology simulations

1) SURFACE CLIMATE

The seasonal cycle of surface temperature and precipitation for the surface hydrology simulations is shown in Fig. 6. The continent in the Northern Hemisphere subtropics is the region of maximum surface temperature for almost all of the year. This is the result of the continent's aridity: When the continent has dried out, the insolation reaching the surface cannot be balanced by evaporation; sensible surface fluxes or net surface longwave radiation, which both increase less rapidly with temperature than evaporation, must balance the net surface shortwave radiation, and the surface warms. The continent's aridity is partly due to the use of a zonally symmetric continent, which eliminates the possibility of zonal advection of water vapor to the continent. The precipitation distribution is biased toward the Southern Hemisphere when the surface hydrology is included (Figs. 6c,d) to a greater extent than in the heat capacity simulations (Figs. 3c,d). For example, in the

December perihelion simulation, the precipitation maximum reaches ~20°S in Southern Hemisphere summer, but only to ~5°N in Northern Hemisphere summer (Fig. 6b). The asymmetry in precipitation is associated with the annual-mean Hadley circulation, which is also substantially asymmetric (Fig. 7).

When the perihelion is changed from December to June, the surface temperature change follows the insolation change in the northern part of the continent (north of ~15°) and over the ocean (Fig. 6b). There is more sensitivity (warming of ~10 K) and less phase lag over the northern part of the continent than over the ocean as a consequence of the differences in the surface energy balance—the lack of evaporative fluxes and the substantially reduced heat capacity. At the southern margin of the continent, the behavior is different: the June perihelion simulation is colder than the December perihelion simulation even in the Northern Hemisphere summer when there is more insolation (with annual-mean cooling of up to 3 K, Fig. 6b). This is because there is more net precipitation in the simulation with June perihelion ($P - E > 0$, Fig. 6d), so the surface energy balance switches from the dry continent regime to one in which evaporation plays a larger role. Desert regions in comprehensive climate model simulations of orbital precession response (e.g., Phillipps and Held 1994; Legrande and Schmidt 2009) have similar changes to those here (cooler surface temperatures when there is more summertime insolation).
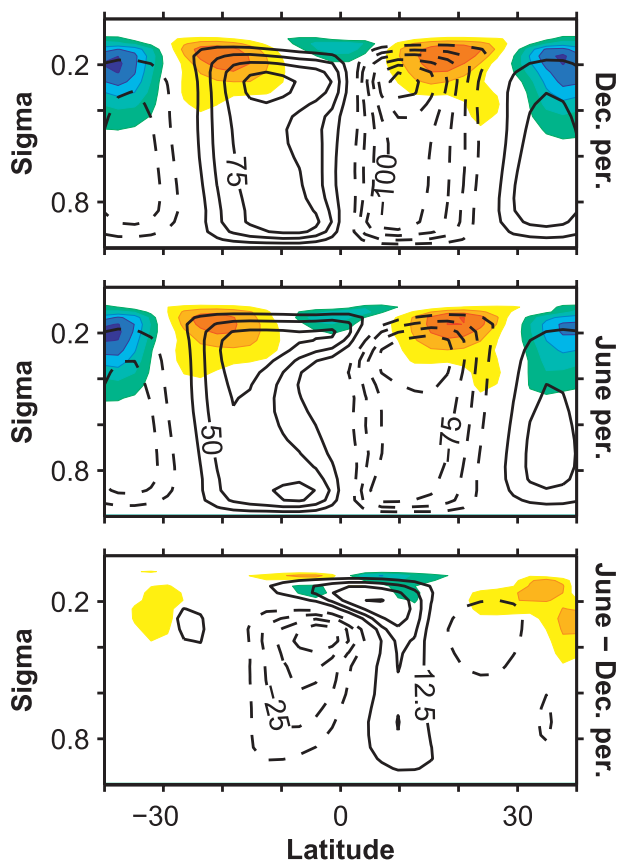
FIG. 4. Annual-mean mass flux streamfunction (contours) with contour interval 25×10^9 kg s^{-1} and eddy angular momentum flux divergence (colors) with contour interval 1.2×10^{-5} m s^{-2} for the heat capacity simulation with (top) December perihelion and (middle) June perihelion. (bottom) Difference in annual-mean streamfunction (contours) with contour interval 12.5×10^9 kg s^{-1} and eddy angular momentum flux divergence (colors) with contour interval 0.6×10^{-5} m s^{-2} between heat capacity simulations with June and December perihelion.

2) HADLEY CIRCULATION

The annual-mean Hadley circulation of the December perihelion simulation is substantially stronger in the Northern Hemisphere than in the Southern Hemisphere and the boundary between the cells is south of the equator in the free troposphere (Fig. 7, top). The annual-mean Hadley circulation weakens in the Northern Hemisphere and changes little in the Southern Hemisphere when perihelion changes from December to June (Fig. 7, bottom). Although the climatological Hadley circulation differs substantially between the surface hydrology and heat capacity simulations, the response to orbital forcing is similar (i.e., the perturbations are not strongly dependent on the mean state). We again consider the seasonal circulations and their changes to understand why the annual-mean Hadley circulation changes this way.

Figure 8 shows the Hadley circulation and its changes with perihelion averaged over two 6-month periods of the year: from June to November and from December to May. The ascending branch of the circulation in the Northern Hemisphere cold season is poleward of that in the corresponding heat capacity simulations (left columns of Figs. 5 and 8). This is likely a consequence of the near-surface moist static energy being altered on the equatorward side of the convergence zone by the stronger mean circulation's moist static energy advection (Schneider and Bordoni 2008); the stronger circulation is, in turn, associated with the greater longwave cooling over the dry continent.

The annual-mean weakening of the Hadley circulation is the result of changes in the monsoonal Hadley circulation in the Northern Hemisphere warm half year. In contrast to the heat capacity simulations, the monsoonal circulation in the Northern Hemisphere cold season does not change substantially between simulations with perihelion in December and June (maximum streamfunction of 320×10^9 and 321×10^9 kg s^{-1}, respectively). In the Northern Hemisphere warm season, the monsoonal Hadley circulation shifts poleward and strengthens (maximum streamfunction increases from 179×10^9 to 222×10^9 kg s^{-1}) when perihelion changes from the December to June solstice (right column of Fig. 5). This change has the same sign as that in the heat capacity simulations, but it is larger in magnitude.

4. Energy balance

The energy balance of the atmosphere and surface is

$$\left\{\frac{\partial \overline{\mathcal{E}}}{\partial t}\right\} + \rho_o c_{po} d \frac{\partial \overline{T}_s}{\partial t} = S_{\text{TOA}} - L_{\text{TOA}}$$
$$- \nabla \cdot \{\overline{\mathbf{u}h}\} - \nabla \cdot \mathbf{F}_o, \quad (4)$$

with total atmospheric energy (neglecting kinetic energy) $\mathcal{E} = c_v T + gz + Lq$, moist static energy $h = c_p T + gz + Lq$, net top-of-atmosphere shortwave radiation S_{TOA}, and net top-of-atmosphere longwave radiation L_{TOA}. The mass-weighted integral over the atmosphere is indicated by $\{\cdot\}$; the zonal and monthly mean is indicated by $\overline{(\cdot)}$ and deviations thereof are indicated by $(\cdot)'$. Note that precipitation does not appear in (4); in contrast, precipitation is a source term in the dry thermodynamic budget and the water vapor budget, so knowledge of regional precipitation is necessary to use them to quantify circulation changes (Merlis and Schneider 2011). If energy storage is negligible, atmosphere–ocean energy flux divergences balance radiation changes: $S_{\text{TOA}} - L_{\text{TOA}} = \nabla \cdot \{\overline{\mathbf{u}h}\} + \nabla \cdot \mathbf{F}_o$. This will be the balance over land
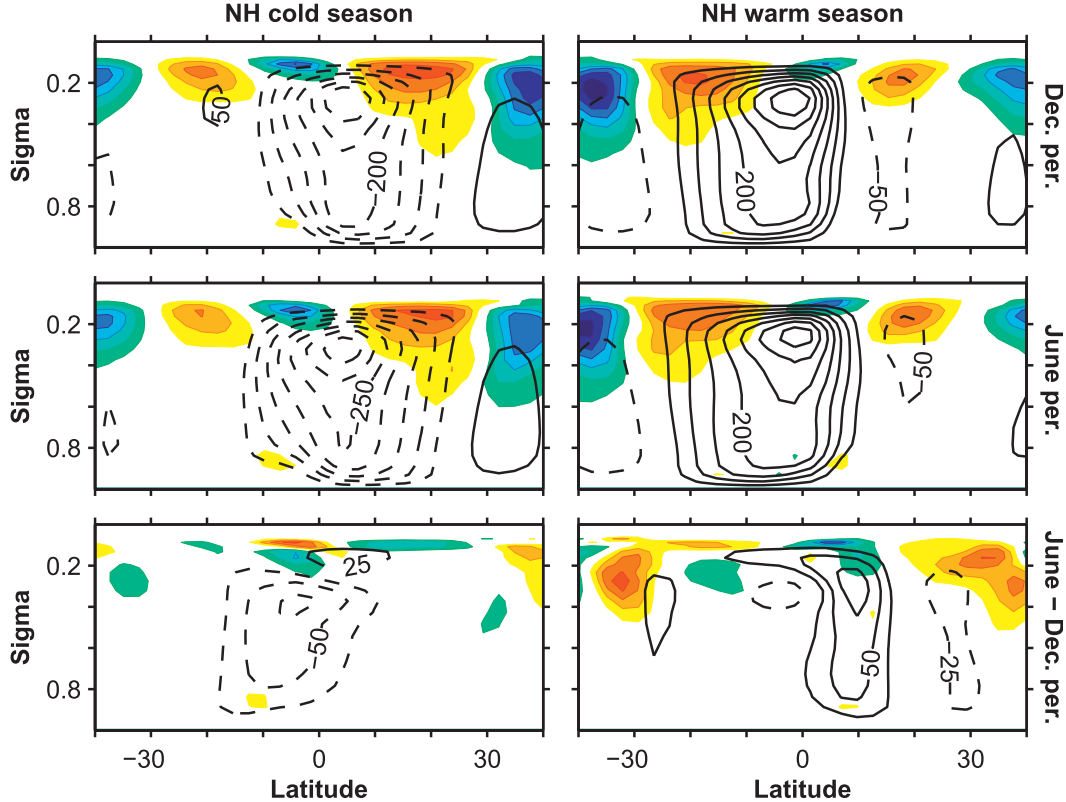
FIG. 5. Mass flux streamfunction (contours) with contour interval 50×10^9 kg s^{-1} and eddy angular momentum flux divergence (colors) with contour interval 1.2×10^{-5} m s^{-2} for the (left) Northern Hemisphere (NH) cold season [Dec–May (DJFMAM)] and (right) NH warm season [Jun–Nov (JJASON)] for heat capacity simulations with (top) December perihelion and (middle) June perihelion. (bottom) Difference in NH cold season and NH warm season streamfunction (contours) with contour interval 25×10^9 kg s^{-1} and eddy angular momentum flux divergence (colors) with contour interval 0.6×10^{-5} m s^{-2} between heat capacity simulations with June and December perihelion.

surfaces where the surface and atmospheric energy storage terms are negligible (the ocean energy flux is also zero).

When there is spatially inhomogeneous energy storage, the energy balance takes the form

$$S_{\text{TOA}} - L_{\text{TOA}} - \mathcal{A}\rho_o c_{po} d\frac{\partial \overline{T}_s}{\partial t} \approx \nabla \cdot \{\overline{\mathbf{u}h}\} + \nabla \cdot \mathbf{F}_o, \quad (5)$$

where

$$\mathcal{A} = \begin{cases} 1, & \text{over oceans} \\ 0, & \text{over land} \end{cases}$$

accounts for the inhomogeneous surface energy storage by neglecting that in land. For simplicity, it is assumed in (5) that energy storage in the atmosphere is negligible; in the simulations, it is a small term and does not have substantial spatial structure. For radiative perturbations such as insolation changes, the perturbation balance becomes

$$\delta(S_{\text{TOA}} - L_{\text{TOA}}) - \mathcal{A}\rho_o c_{po} d\delta\left(\frac{\partial \overline{T}_s}{\partial t}\right) \approx \delta\nabla \cdot \{\overline{\mathbf{u}h}\} + \delta\nabla \cdot \mathbf{F}_o. \quad (6)$$

We call the left-hand side of (6) the "effective" radiative perturbation δR_{eff}, which includes the inhomogeneous surface energy storage term. It is the component of the radiative perturbation that is uncompensated by the surface energy storage, so the atmospheric and oceanic energy flux divergences must balance it. In the idealized GCM simulations with fixed Q-flux, the effective radiative perturbation must be balanced by the atmospheric energy flux divergence. Chou and Neelin (2003) presented observational analyses and simulations of the net input of energy into the atmospheric column (denoted F^{net}), which only differs from R_{eff} in that it includes the ocean heat flux convergence. The central modification of the inhomogeneous heat capacity is then to produce a jump in the effective radiative perturbation at the edge of the continent. There, the balance switches from the
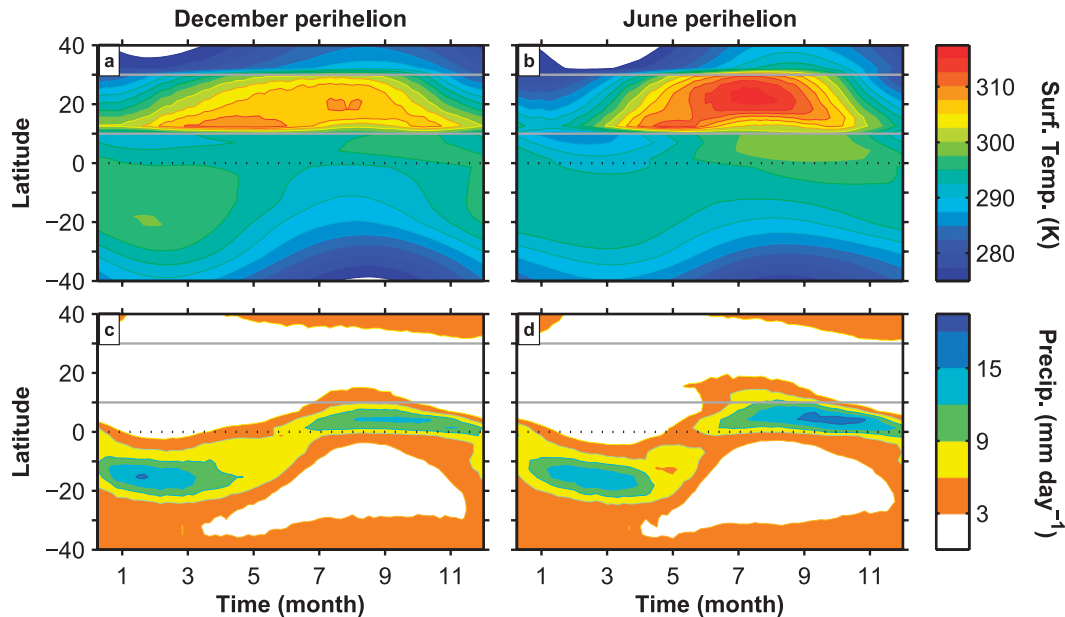
FIG. 6. (a),(b) Seasonal cycle of surface temperature and (c),(d) seasonal cycle of precipitation for surface hydrology simulations with perihelion in (a),(c) December and (b),(d) June. The contour interval is 2.5 K for surface temperature and 3 mm day^{-1} for precipitation, and the boundaries of the continent are shown in gray.

continental regime with no energy storage, in which the atmospheric energy flux divergence must balance the radiative perturbation, to the oceanic regime, in which surface energy storage may balance essentially all of the radiative perturbation, and the atmospheric energy flux divergence does not need to change to balance the top-of-atmosphere energy budget. Knowledge of the effective radiative perturbation does not directly constrain the mean mass circulation as both gross moist stability (cf. Part I) and eddy moist static energy flux divergence can change. Hsu et al. (2010) performed a similar analysis to understand the response of zonally asymmetric circulations to orbital precession.

Figure 9 shows the change in the energy balance of the sum of the atmosphere and surface in the Northern Hemisphere summer in response to perihelion changing from December to June. The effective net radiation change is large and positive over the subtropical continent but is smaller over the adjacent regions with greater heat capacity. The atmospheric moist static energy flux divergence, which must balance the effective net radiation changes, does this by increased mean-flow energy flux divergence on the equatorward side of the continent and through increased eddy energy flux divergence on the poleward side of the continent. Figure 9 does not show the atmospheric energy storage, which accounts for most of the difference between the atmospheric energy flux divergence and the effective radiation perturbation; it does not vary strongly in latitude. There is

also a residual ($\lesssim 15$ W m^{-2}) at the continent boundary that may be the result of the different discretization used to compute the divergence in the GCM and in the analysis of the simulation results.

Note the similarity in changes in the top-of-atmosphere energy balance between heat capacity simulations and surface hydrology simulations (Fig. 9, left and right). These simulations have quite different surface climates (e.g., the annual-mean surface temperature in the continent region is ~295 K in the heat capacity simulations compared to ~305 K in the surface hydrology simulations, Figs. 3 and 6) and have oppositely signed changes in surface temperature at the southern boundary of the continent when perihelion is varied. Biasutti et al. (2009) also found that the sign of the surface temperature gradient change is not predictive of the sign of the circulation change in simulations of African climate change. In spite of the oppositely signed surface temperature changes, the response to orbital precession is similar in terms of the top-of-atmosphere energy balance and the mean atmospheric circulation. The similarity between the changes in the top-of-atmosphere energy balance in the two sets of simulations is due in part to the lack of cloud and surface albedo feedbacks, so the top-of-atmosphere energy balance in comprehensive simulations likely has more sensitivity to the land surface treatment.

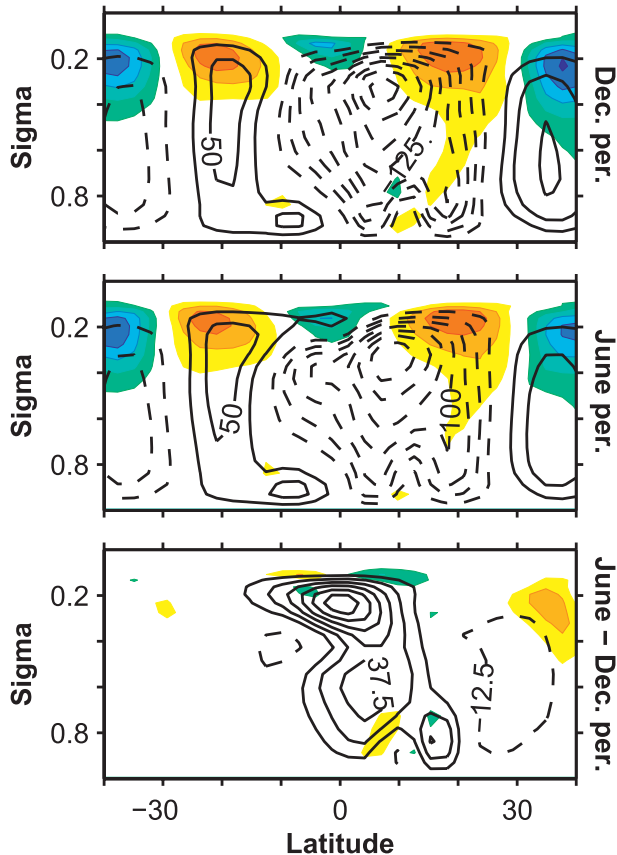Why is it that the ascending branch of the winter cell shifts farther poleward into the summer hemisphere and

FIG. 7. Annual-mean mass flux streamfunction (contours) with contour interval 25×10^9 kg s^{-1} and eddy angular momentum flux divergence (colors) with contour interval 1.2×10^{-5} m s^{-2} for the surface hydrology simulation with (top) December perihelion and (middle) June perihelion. (bottom) Difference in annual-mean streamfunction (contours) with contour interval 12.5×10^9 kg s^{-1} and eddy angular momentum flux divergence (colors) with contour interval 0.6×10^{-5} m s^{-2} between surface hydrology simulations with June and December perihelion.

the cell strengthens when perihelion moves from December to June in simulations with a Northern Hemisphere continent (Figs. 5 and 8)? The near-surface moist static energy maximum determines the boundary between the summer and cross-equatorial, monsoonal Hadley circulation [under conditions outlined in the appendix, which reviews the argument of Privé and Plumb (2007)]. Figure 10 shows that the moist static energy maximum moves poleward when the perihelion is in June and, consistent with the argument of Privé and Plumb, the boundary of the ascending branch of the monsoonal Hadley circulation nearly coincides with it. We note that the moist static energy distribution is not solely a function of the top-of-atmosphere radiation perturbation. The aquaplanet simulations (Part I) provide a concrete counterexample: The convergence zone

boundaries did not shift when perihelion was varied. This shows that the meridional structure of the insolation changes associated with orbital precession is not sufficient to determine the position of the moist static energy maximum. Here, the presence of the inhomogeneous surface heat capacity provides meridional structure that shifts the moist static energy maximum northward when the perihelion is in the Northern Hemisphere summer. This is because the region of low heat capacity in the Northern Hemisphere subtropics is constrained to have balanced surface fluxes on short time scales. So, insolation changes reaching the surface are rapidly balanced by surface enthalpy fluxes that increase the near-surface moist static energy. In contrast, over the oceanic region insolation changes are balanced by both surface fluxes and surface energy storage. Because the near-surface moist static energy increases more rapidly over the continent, the convergence zone shifts into the Northern Hemisphere in early summer when perihelion is in June (Fig. 10). The near-surface moist static energy also decreases more rapidly over the continent at the end of the Northern Hemisphere summer, when the sign of the insolation change is reversed; however, at this point, the convergence zone has already moved over the oceanic region (Fig. 10), so the circulation boundary is not sensitive to the more rapid changes in the continent region. Note that the circulation boundary is in the Northern Hemisphere for a larger fraction of the year in the simulations with June perihelion than in the simulations with December perihelion because of the combination of the more rapid onset in the beginning of the warm season and the similar decay at the end of the warm season (Fig. 10).

The convergence zone and near-surface moist static energy maximum differ by up to ~10° in the early Northern Hemisphere summer in the December perihelion surface hydrology simulations (Fig. 10). That the arguments of Privé and Plumb (2007) do not hold as closely in the surface hydrology simulations is not unexpected, as the surface becomes very dry (Fig. 6) and shallow circulation cells are present (Fig. 8). The situation is similar to that over several of Earth's continents, which have (dry) potential temperature maxima and shallow circulations (Nie et al. 2010). The factors governing the interactions between the thermodynamic state of the atmosphere and shallow and deep circulations have not been fully laid bare, but the arguments of Privé and Plumb assume that quasi-equilibrium holds and, implicitly, the vertical structure of the circulation is deep.

In Part I, changes in the atmosphere's gross moist stability were important in determining the changes in Hadley circulation strength when perihelion varied. In
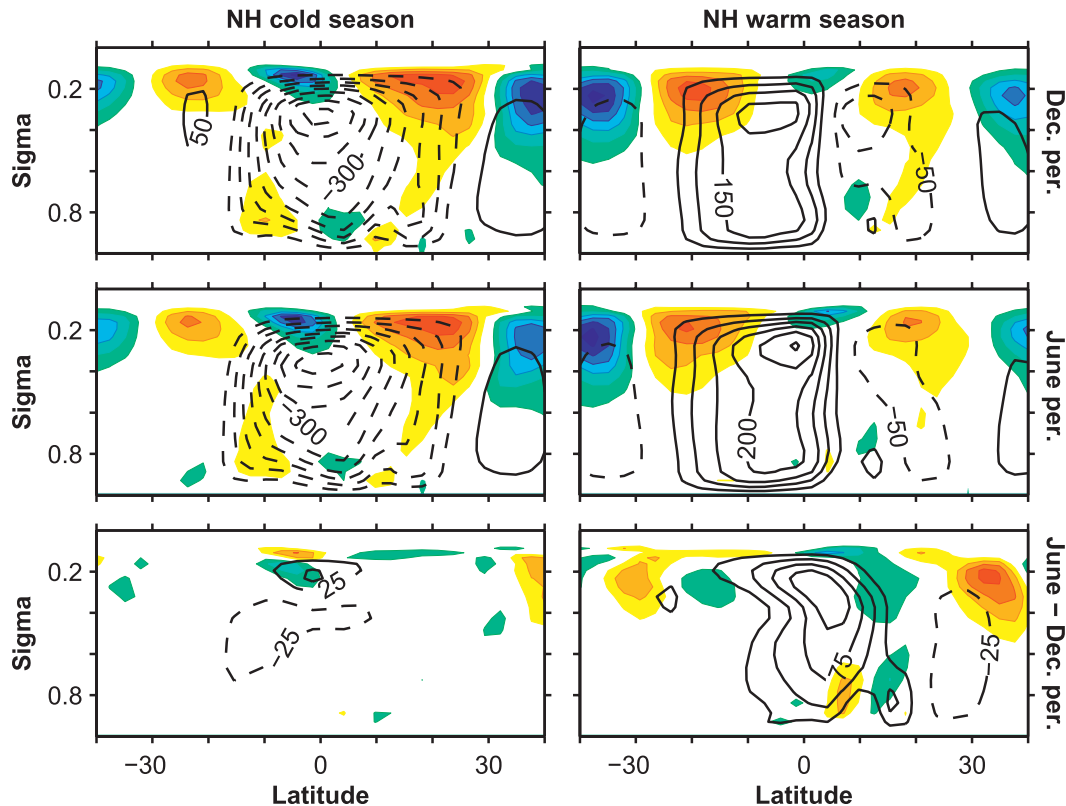
FIG. 8. Mass flux streamfunction (contours) with contour interval 50×10^9 kg s^{-1} and eddy angular momentum flux divergence (colors) with contour interval 1.2×10^{-5} m s^{-2} for the (left) Northern Hemisphere (NH) cold season (DJFMAM) and (right) NH warm season (JJASON) for surface hydrology simulations with (top) December perihelion and (middle) June perihelion. (bottom) Difference in NH cold season and NH warm season streamfunction (contours) with contour interval 25×10^9 kg s^{-1} and eddy angular momentum flux divergence (colors) with contour interval 0.6×10^{-5} m s^{-2} between surface hydrology simulations with June and December perihelion.

the simulations here, it seems that this is a secondary factor.[1] The strengthening of the Northern Hemisphere warm season monsoonal Hadley cell results from the more rapid transition in the beginning of the season and the overall longer time that the convergence zone is in the

---

[1] The convergence zone location estimate of Privé and Plumb (2007) and gross moist stability estimate of Held (2001b) both depend on the near-surface moist static energy distribution. One might expect the increase in moist static energy that is responsible for the poleward shift in the convergence zone to also be associated with an increase in the gross moist stability, which would tend to weaken the circulation mass flux. However, the functional form of the dependence on the moist static energy is different for the two estimates: the convergence zone location estimate depends on the maximum near-surface moist static energy, while the Held estimate for the gross moist stability depends on its meridional gradients. If the maximum in moist static energy shifts in a region of weak gradients, the convergence zone location can shift without a substantial change in gross moist stability. This appears to be the case in the heat capacity simulations here, although many factors can affect the gross moist stability.

Northern Hemisphere (Fig. 10). That the convergence zone is north of the equator on average is not what one would expect from considering the insolation distribution alone because the bright summer is also shorter (Fig. 2 of Part I); to understand the convergence zone location, one must consider the interaction between the insolation and surface properties, which can lead to sharper meridional gradients in the near-surface moist static energy at the beginning of the season when the convergence zone transitions between the hemispheres.

5. Annual-mean circulation changes

How can seasonal changes due to orbital precession lead to rectified annual-mean Hadley circulation changes? If the year is divided into warm and cold half years as we have, the annual-mean circulation can change if both half years have similarly signed changes. Alternatively, if one of the half years has changes and the other does not, this will lead to rectification. In this case, one must explain why the circulation is sensitive to
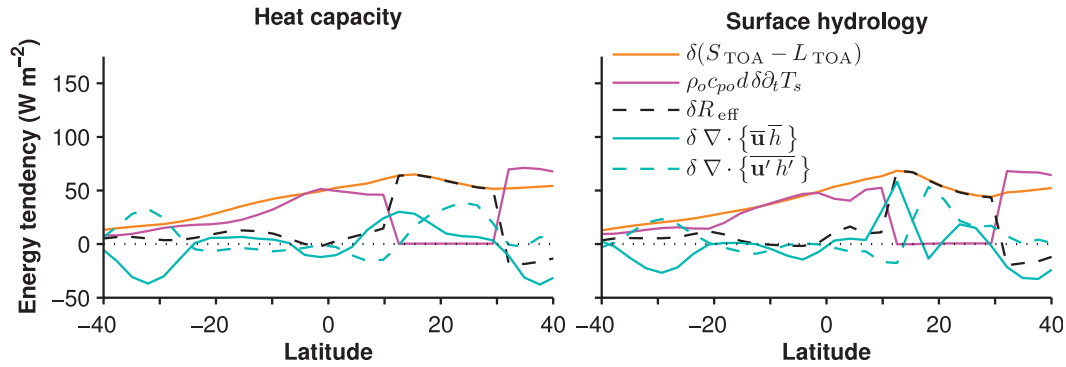
FIG. 9. June–August (JJA) atmosphere–ocean energy balance difference between (left) heat capacity and (right) surface hydrology simulations with June and December perihelion.

insolation changes in one of the half years but not the other since the insolation changes are present in both half years with opposite sign.

A concrete example of this second type of rectification is given by threshold behavior. For example, the model of Plumb and Hou (1992) has a regime transition between a thermal equilibrium state with no mean meridional circulation (or a viscous circulation in numerical simulations) and an angular momentum-conserving circulation as off-equatorial thermal forcing is increased. But it is not clear that the dynamics described in Plumb and Hou are relevant for Earth's monsoon circulations since the threshold relies on there being no thermal gradients at the equator, a condition that is not satisfied in Earth's climate.

The aquaplanet simulations in Part I are an example of the first type of rectification. The Hadley circulation had same-signed changes in the two half years: the warm season had weaker cross-equatorial Hadley circulation mass fluxes when the insolation increased with perihelion coinciding with that season; because the insolation

changes in the cold season are opposite in sign to those of the warm season, the cold season mass fluxes strengthened when there was less insolation. The weaker warm half-year and stronger cold half-year Hadley circulation do not cancel because the sign of the circulation climatology is reversed (streamfunction anomalies in both seasons are negative). In the annual mean, this leads to Hadley circulation changes centered on the equator.

The Hadley circulations of the simulations presented here are rectified by changes that occur solely in one season. In this section, we explain why the Hadley circulation changes are confined to the hemisphere of the ascending branch (in both half years in the heat capacity simulations and in the Northern Hemisphere warm season in the surface hydrology simulations). This occurs as the result of a previously undiscussed nonlinearity associated with the changing regime of the angular momentum balance. The approximate angular momentum balance of the free troposphere, neglecting vertical momentum advection by the mean flow, is
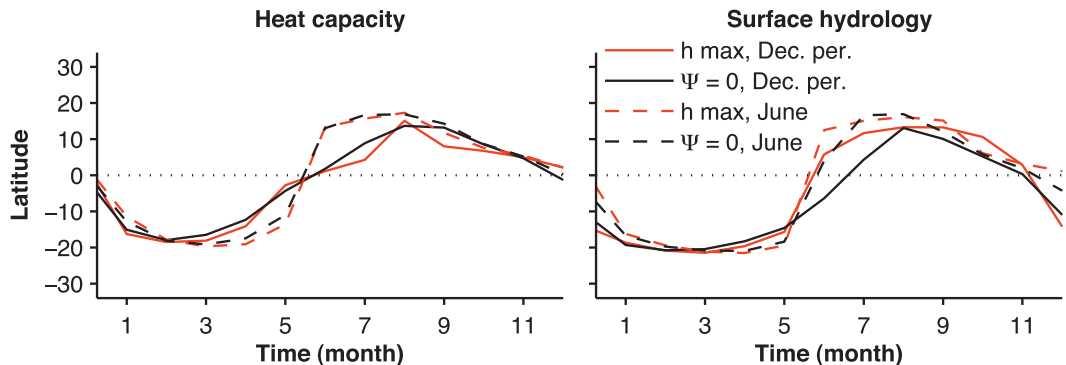

FIG. 10. Seasonal cycle of the latitude of the maximum near-surface moist static energy h (on the $\sigma = 0.93$ model level; red lines) and the convergence zone between the summer and cross-equatorial monsoonal Hadley cells (defined as the streamfunction zero on the $\sigma = 0.67$ model level; black lines) for (left) heat capacity and (right) surface hydrology simulations with perihelion in December (solid lines) and June (dashed lines).

$(f + \bar{\zeta})\bar{v} = f(1 - \text{Ro})\bar{v} \approx \mathcal{S}$, with local Rossby number $\text{Ro} = -\bar{\zeta}/f$, eddy momentum flux divergence $\mathcal{S}$, and other symbols with their usual meaning (Walker and Schneider 2006; Schneider 2006). The local Rossby number characterizes whether the angular momentum balance of the circulation is close to the angular momentum-conserving limit ($\text{Ro} \rightarrow 1$) or to the limit in which the circulation is slaved to the eddy momentum flux divergence ($\text{Ro} \rightarrow 0$). The local Rossby number is evaluated in the GCM simulations as the ratio of the Eulerian mean streamfunction associated with mean-flow momentum fluxes to the total Eulerian mean streamfunction (Part I).

The Rossby number at the streamfunction maximum (i.e., the extremum of the Southern Hemisphere circulation cell) varies from ~1 in Northern Hemisphere summer to ~0 in Northern Hemisphere winter (Fig. 11). In the angular momentum-conserving regime ($\text{Ro} \sim 1$), the monsoonal Hadley cell responds directly to thermodynamic or energetic changes, such as precession-forced changes in the insolation distribution. In contrast, the Hadley cell does not respond directly to changes in the insolation distribution in the low Rossby number regime ($\text{Ro} \sim 0$). Therefore, the Hadley cell sensitivity to the precession forcing varies over the course of the year because of the time dependence of the Hadley cell's angular momentum balance (i.e., the seasonal cycle of the cell's Rossby number). In addition to the energetic changes that occur when the circulation is near the angular momentum-conserving limit, changes in the Rossby number and eddy momentum fluxes can affect the Hadley circulation strength, though these do not appear to be critical here.

The maximum streamfunction value in Northern Hemisphere summer does not change substantially with perihelion in the heat capacity simulations, as noted in section 3; the Hadley circulation changes are primarily associated with shifts in the northern extent of the cross-equatorial circulation and occur between the streamfunction maximum and northern boundary of the cell (Fig. 5). Changes in the eddy component of the streamfunction and Rossby number are also small when perihelion is varied in the heat capacity simulations (Fig. 11). Where there are annual-mean circulation changes, the energetic changes during the time of year when the circulation is near the angular momentum-conserving limit are important. Similarly, in the surface hydrology simulations the maximum streamfunction value increases in Northern Hemisphere summer when perihelion changes from December to June, while the eddy component of the streamfunction changes little or weakens, with a corresponding increase in the Rossby number (Fig. 11). Therefore, it appears that the energetic

changes in Northern Hemisphere summer are the primary mechanism that changes the circulation strength. These changes in Northern Hemisphere summer affect the annual-mean circulation because the regime of the angular momentum balance in the rest of the year is such that the circulation does not respond directly to energetic changes.

An alternative to examining the Hadley circulation at the latitude of the maximum streamfunction is to consider a fixed subtropical latitude. There, the ascending branch of the monsoonal Hadley circulation in summer is close to the angular momentum-conserving limit ($\text{Ro} \sim 1$), while the descending branch of the monsoonal Hadley circulation in winter is typically of intermediate Rossby number ($\text{Ro} \sim 0.5$). In this case, the angular momentum balance is a three-way balance between the mean-flow nonlinear momentum advection, the Coriolis force, and the eddy angular momentum flux divergence, so energetic considerations do not directly determine the circulation strength (Schneider 2006; Schneider et al. 2010). Thus, there is an asymmetry between the ascending and descending branches of the Hadley circulation in terms of the momentum balance: the monsoonal Hadley circulation in the warm season will change in response to energetic changes but the Hadley circulation in the cold season is not free to respond directly to thermodynamic changes as it is influenced by eddies. Evaluating the GCM simulations at fixed subtropical latitudes is qualitatively similar to Fig. 11 but is more sensitive to averaging conventions.

Though the seasons that give rise to the annual-mean Hadley circulation changes is different in Part I and in the simulations here, the important dynamical regime is that of the high Rossby number limit in both cases. As such, the spatial structure and time dependence of the Rossby number are generally important parameters in developing estimates for perturbations to the Hadley circulation.

6. Synthesis of monsoonal Hadley circulation dynamics

This section is devoted to a summary of the factors that enter a perturbation theory for the monsoonal Hadley circulation. In the aquaplanet simulations in Part I, changes in gross moist stability were central to changes in the strength of the Hadley circulation. In the simulations with a subtropical continent presented here, changes in the poleward boundary of the monsoonal circulation and the role of inhomogeneous surface energy storage are important. In this section, we summarize the factors that affect the monsoonal Hadley circulations in our idealized settings. There are several
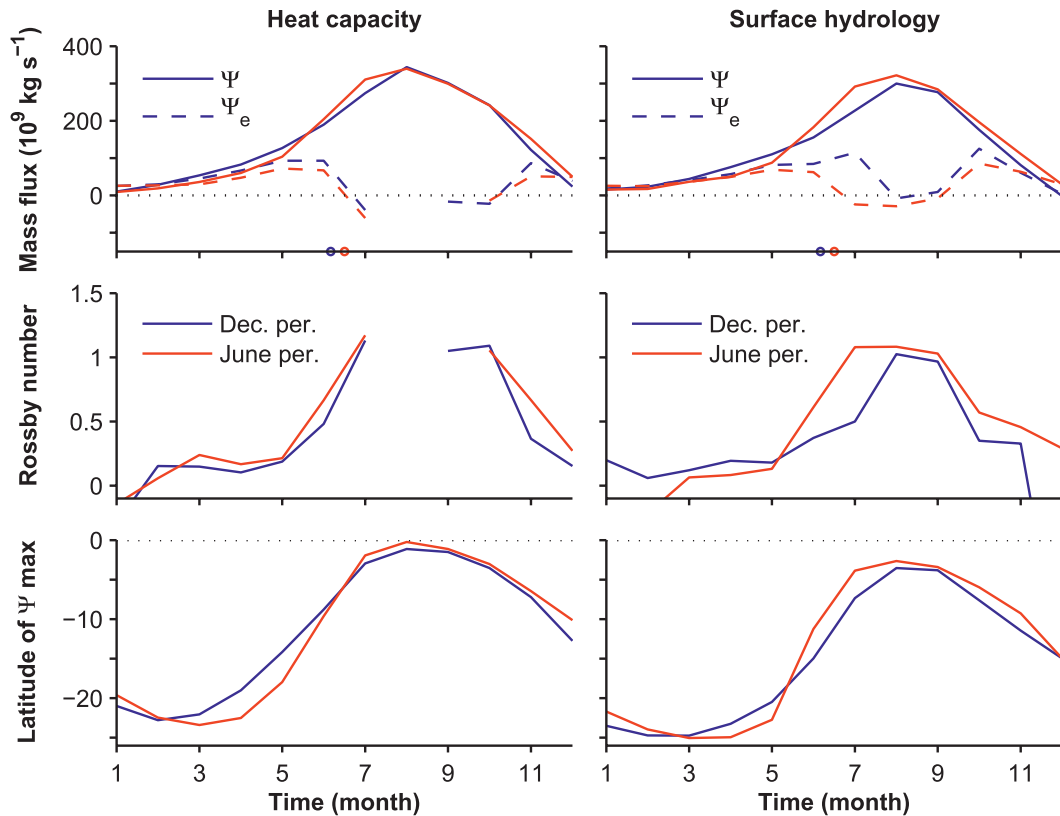
FIG. 11. (top) Seasonal cycle of the streamfunction (solid) and eddy component of the streamfunction (dashed; see Part I for definition) evaluated on the $\sigma = 67$ model level at the latitude of streamfunction maximum for simulations with perihelion in June (red) and December (blue). The eddy component of the streamfunction is not plotted when the streamfunction maximum is within 4° of the equator because it is ill defined when the Coriolis parameter approaches zero. Markers on the horizontal axis indicate the time of year of the Northern Hemisphere summer solstice. (middle) Seasonal cycle of the vertically averaged Rossby number $\langle Ro \rangle$ (see Part I for definition) above the $\sigma = 67$ model level (the Rossby number is not plotted for $|\Psi| < 20 \times 10^9$ kg s^{-1} as it is ill defined for near-zero values of the streamfunction). (bottom) Seasonal cycle of the latitude of maximum streamfunction on the $\sigma = 0.67$ model level. (left) Heat capacity simulation results and (right) surface hydrology simulation results.

common elements in the discussion here, which is focused on moist dynamics, and the discussion presented in Schneider and Bordoni (2008), which is focused on dry dynamics.

(i) The perturbation top-of-atmosphere energy balance and the energy storage determine the requisite change in the total (mean and eddy) energy flux divergence.

(ii) Given the changes in the transient eddy energy flux divergence, the mean flow component of the energy flux divergence is known. We have not addressed the eddy component of energy fluxes in low latitudes here, though the eddy dry static energy fluxes are generally small because of weak temperature gradients in the free troposphere and eddy moisture fluxes are generally downgradient (Schneider et al. 2006; Peters et al. 2008; Couhert et al. 2010).

(iii) The convergence zone location (the boundary between the summer and cross-equatorial, monsoonal Hadley cells) determines whether the summer or winter Hadley circulation accounts for the changing mean-flow energy fluxes. Changes in the convergence zone location are, in turn, related to changes in the near-surface moist static energy distribution under the conditions when the argument of Privé and Plumb (2007) holds. The perturbation near-surface moist static energy depends on the structure of the radiative perturbation and the spatial structure of the surface heat capacity (section 4). We illustrate this with a simple conceptual model: Assuming that the precession-forced change in surface shortwave radiation is balanced only by changes in surface energy storage, with spatially varying heat capacity, and perturbation surface enthalpy fluxes that depend linearly on the perturbation

surface temperature (e.g., Merlis and Schneider 2011), the perturbation surface energy budget is $\rho_o c_{po} d \delta \partial_t T_s = \delta S_{surf} - \beta \delta T_s$. If the perturbation surface moist static energy δh_s is proportional to the perturbation surface enthalpy fluxes ($\delta h_s \sim \beta \delta T_s$), it will have substantial spatial variation near the continent boundary because the perturbation enthalpy flux is small where the heat capacity is large and the perturbation enthalpy flux is large where the heat capacity is small. In contrast, when this model is applied to an aquaplanet, with uniform surface heat capacity, spatial variation in the perturbation moist static energy only arises from the planetary-scale precession forcing. This conceptual model is only a partial description of the factors affecting the near-surface moist static energy because it can also be modified by atmospheric moist static energy advection (e.g., Chou et al. 2001; Su and Neelin 2005).

(iv) The change in the mean-flow energy flux divergence can be balanced by changes in the mean-flow mass flux or by changes in the gross moist stability (e.g., Held 2001a; Part I). The Held (2001b) estimate broadly accounts for the spatial variations in the gross moist stability, although the factors that determine the gross moist stability in regions of ascent remain to be elucidated.

The energetic framework applies in the high Rossby number limit since the angular momentum balance $[f(1 - Ro)\bar{v} \approx \mathcal{S}$, with $Ro \to 1$ and $\mathcal{S} \to 0]$ is degenerate (Walker and Schneider 2006; Schneider 2006). So, a complete description of the Hadley circulation changes must also account for the factors on which the time-dependent Rossby number Ro and eddy momentum flux divergence $\mathcal{S}$ depend. We have largely left this unaddressed, but we briefly discuss these issues here.

In the intermediate and low Rossby number regimes of the angular momentum balance, extratropical eddies can influence the Hadley circulation strength. In the heat capacity simulations presented here, the changes in the eddy-driven component of the streamfunction were not crucial (Fig. 11), which may be the result of the weak dependence of extratropical eddies on meridional temperature gradients (Schneider and Walker 2008; O'Gorman and Schneider 2008) and possibly changes in duration and intensity of insolation gradients that offset each other [e.g., extratropical eddy quantities shown in Jackson and Broccoli (2003) have weaker changes with precession than with obliquity]. A systematic examination of the response of extratropical eddies to orbital forcing in the framework of current theoretical developments (Schneider et al. 2010; O'Gorman 2011) is

warranted. In addition to extratropical eddies, barotropic instability in the tropics can affect the Hadley circulation momentum balance.

The factors that control the seasonal cycle of the Rossby number are important as this is central to the mechanism that gives rise to the annual-mean circulation changes discussed here (section 5). Schneider and Bordoni (2008) presented two mechanisms that can give rise to a rapid seasonal transition between low and high Rossby number regimes: (i) the interaction between the near-surface temperature advection and the position of the convergence zone and (ii) eddy shielding by easterly winds that develop as convergence zones move off of the equator, for which there has been progress in developing conceptual representations of the interaction between the mean meridional circulation and eddy momentum fluxes (Sobel and Schneider 2009). We have not assessed the role of these mechanisms in determining the seasonality of the reference-simulation Rossby number, nor their changes with perihelion, as empirically this does not seem to be quantitatively important.

7. Conclusions

In this study and in a companion paper (Part I), the factors affecting the Hadley circulation seasonal and annual-mean response to orbital precession have been assessed in a range of idealized GCM simulations. In the summer season, the cross-equatorial monsoonal Hadley circulation responds directly to energetic changes, such as those due to perturbations in the top-of-atmosphere radiation, if the momentum balance of the circulation is close to angular momentum conserving. In the annual mean, Hadley circulation changes can depend on a variety of factors, as the angular momentum balance has a seasonal cycle that makes different regimes important in different parts of the seasonal cycle.

In Part I, the monsoonal Hadley circulation mass flux decreased when the perihelion was varied such that there was more sunlight in the monsoon season. This result is counterintuitive as it contradicts expectations based on land–sea breeze conceptions of large-scale circulations or off-equatorial angular momentum-conserving circulation theories with fixed gross stability (Lindzen and Hou 1988). We showed that this is a consequence of the energy balance constraining the product of the mass flux and the gross moist stability, rather than the mass flux itself, and the rapid increase of the gross moist stability in response to insolation changes. While the strength of the circulation changed, there were no substantial changes in the convergence zone position in the aquaplanet simulations.

In this study, the monsoonal Hadley circulation mass flux increased when the perihelion occurred in the hemisphere with a subtropical continent. The perturbation energy budget is different in this case because of the presence of inhomogeneity in the surface heat capacity. The low heat capacity of the land dictates that radiative perturbations are balanced by surface fluxes to the atmosphere; ocean regions, in contrast, can balance radiative perturbations by surface energy storage. Thus, the required perturbation atmospheric energy flux divergence varies substantially near the continent boundary. One can think of the difference between the top-of-atmosphere radiation changes and the surface energy storage as the ''effective'' radiation perturbation (the component of the radiation changes that is uncompensated by ocean heat uptake), which the atmospheric circulation must balance. These top-of-atmosphere energy budget considerations do not depend in detail on the surface climate, as comparing the heat capacity and surface hydrology land models makes clear (Fig. 9).

In the subtropical continent simulations, the monsoonal Hadley circulation in the summer of the hemisphere with a continent underwent a poleward shift in response to changing perihelion phase such that the summer was brightened. The argument of Privé and Plumb (2007) that relates the position of the convergence zone to the near-surface moist static energy maximum accounted for the simulated changes in convergence zone location, though there is some discrepancy in surface hydrology simulations, as expected because moist quasi-equilibrium does not hold over arid surfaces. The changes in the surface moist static energy distribution that lead to a more rapid transition of the convergence zone into the Northern Hemisphere summer were associated with the lower heat capacity of the continent. The simulation results have the counterintuitive behavior that the convergence zone spends more time in the Northern Hemisphere summer when that summer is bright and short—at odds with what one would expect from solely considering the insolation.

The annual-mean Hadley circulation changes in both the simulations of this study and the aquaplanet simulations of Part I are the result of changes in the circulation during the season when it is near the angular momentum–conserving limit. In Part I, the annual-mean Hadley circulation changes were the result of the combination of monsoonal Hadley circulation changes in both solstice seasons. In this study, the annual-mean Hadley circulation changes are primarily associated with the summer season due to a previously undocumented mechanism in which the annual mean can be affected by changes in one season because the Rossby number

depends on season. Changes in the fraction of the year that the convergence zone was located in each hemisphere are an important factor in the annual-mean changes in these simulations. When perihelion is at the Northern Hemisphere summer solstice, the maximum in surface moist static energy shifts north in the early part of the Northern Hemisphere summer, and the atmospheric circulation follows. This gives rise to annual-mean Hadley circulation changes associated with the longer time that the Hadley circulation is in the Northern Hemisphere, together with the lack of sensitivity to changes in winter (section 5). The changes in the warm half of the year are not offset by opposing changes in the cold half of the year because of the time dependence of the Rossby number: In the winter hemisphere (in the descending branch of the monsoonal Hadley cell), the Rossby number is intermediate ($\sim$0.5), so energetic considerations do not directly affect the Hadley cell strength. In the summer hemisphere (in the ascending branch of the cross-equatorial winter Hadley cell), the Rossby number is high ($\sim$1), so energetic considerations directly influence the Hadley cell strength. Note that this mechanism depends on the different regimes in the angular momentum balance over the course of the year, so it cannot be captured by axisymmetric models [see Bordoni and Schneider (2010) for a comparison of axisymmetric and eddy-permitting GCMs]. The seasonality of the Rossby number may also be relevant in determining greenhouse gas–forced Hadley circulation changes.

A consequence of the importance of the top-of-atmosphere energy balance on the atmospheric circulation is that the circulation dynamics and their changes in response to precession are largely similar between the simulations in which land is modeled as a region of low heat capacity (with a saturated surface) or in which the effects of surface hydrology are also included, in spite of the differences in the surface climate (Figs. 3 and 6). The atmospheric dynamics depend on the surface properties to the extent that they (i) determine the gross moist stability, which was of primary importance in Part I, and (ii) help set the near-surface moist static energy maximum with which the convergence zone is collocated. The argument of Privé and Plumb (2007) for the convergence zone location does not generally extend to the surface hydrology simulations, which violate some of its assumptions. The relationship between the thermodynamic state of the surface and atmosphere and the mean atmospheric circulation in the dry continent regime merits additional investigation.

A complete quantitative understanding of the Hadley circulation changes depends on the factors outlined in section 6; several of which warrant further examination.

In addition, the consequences of aspects of the climate system that are omitted in these idealized simulations (cloud and surface albedo feedbacks, ocean heat transport changes, and orographic effects) and of simulations of intermediate perihelion values in the precession cycle are important areas of future study because of their relevance to paleoclimate proxy records. The tropical circulation changes examined here and in Part I have implications for the response of precipitation to orbital precession, which we report in Merlis et al. (2013b).

APPENDIX

The Relationship between the Convergence Zone Location and the Surface Moist Static Energy Maximum of Privé and Plumb

Privé and Plumb (2007) proposed a relationship between convergence zone location and the surface moist static energy maximum. The argument is an application of the relationship between surface moist entropy and vertical zonal wind shear derived by Emanuel (1995) and is reproduced here.

First, thermal wind balance is expressed in specific volume α as

$$\frac{\partial u}{\partial p} = \frac{1}{f}\frac{\partial \alpha}{\partial y}. \tag{A1}$$

Second, one of the Maxwell relations is used to express the meridional specific volume gradient in terms of temperature and moist entropy gradients,

$$\left(\frac{\partial \alpha}{\partial y}\right)_p = \left(\frac{\partial T}{\partial p}\right)_{s*}\frac{\partial s*}{\partial y}, \tag{A2}$$

where $s*$ is the saturation moist entropy and $(\cdot)*$ indicates a saturation quantity (Emanuel 1994). In surface quasi equilibrium, the surface moist entropy s_b determines that of the free troposphere: $s* = s_b$. Putting together these relationships, the thermal wind balance

can be reexpressed in terms of the moist adiabatic lapse rate and the surface moist entropy gradient,

$$\frac{\partial u}{\partial p} = \frac{1}{f}\left(\frac{\partial T}{\partial p}\right)_{s*}\frac{\partial s_b}{\partial y}. \tag{A3}$$

The surface moist entropy s_b is closely related to the surface moist static energy h_b: $\delta h_b \approx T_b \delta s_b$, so

$$\frac{\partial u}{\partial p} = \frac{1}{f}\left(\frac{\partial T}{\partial p}\right)_{s*}\frac{1}{T_b}\frac{\partial h_b}{\partial y}. \tag{A4}$$

If the circulation is angular momentum conserving, the convergence zone at the boundary of the cell will be in region of no shear ($\partial_p u \approx 0$), as this is a region in which there is no meridional momentum advection and vertical momentum advection homogenizes the vertical momentum distribution if the cell boundary is vertical. The condition on the vertical boundary of the circulation results from transforming between the streamfunction coordinate (the angular momentum of the flow is conserved along streamlines) and pressure coordinates

$$\frac{\partial M}{\partial \Psi} = \frac{\partial M}{\partial p}\frac{\partial p}{\partial \Psi} = 0, \tag{A5}$$

where $M = (\Omega a \cos\phi + u)a \cos\phi$ is the absolute angular momentum.

As the left-hand side of (A4) is zero, this implies that either $(\partial_p T)|_{s*} = 0$ or $\partial_y h_b = 0$. The moist adiabatic lapse rate is not zero, so the poleward boundary of the Hadley circulation occurs where $\partial_y h_b = 0$. Therefore, the maximum in h_b determines the convergence zone at the boundary of the cell (i.e., the region of ascent).

REFERENCES

Biasutti, M., A. H. Sobel, and S. J. Camargo, 2009: The role of the Sahara low in summertime Sahel rainfall variability and change in the CMIP3 models. *J. Climate,* **22,** 5755–5771.

Bordoni, S., 2007: On the role of eddies in monsoonal circulations: Observations and theory. Ph.D. dissertation, University of California, Los Angeles, 195 pp.

——, and T. Schneider, 2008: Monsoons as eddy-mediated regime transitions of the tropical overturning circulation. *Nat. Geosci.,* **1,** 515–519.

——, and ——, 2010: Regime transitions of steady and time-dependent Hadley circulations: Comparison of axisymmetric and eddy-permitting simulations. *J. Atmos. Sci.,* **67,** 1643–1654.

Braconnot, P., and Coauthors, 2007: Results of PMIP2 coupled simulations of the Mid-Holocene and Last Glacial Maximum—Part 2: Feedbacks with emphasis on the location of the ITCZ and mid- and high latitudes heat budget. *Climate Past,* **3,** 279–296.

Chao, W. C., and B. Chen, 2001: The origin of monsoons. *J. Atmos. Sci.,* **58,** 3497–3507.

Chou, C., and J. D. Neelin, 2003: Mechanisms limiting the northward extent of the northern summer monsoons over North America, Asia, and Africa. *J. Climate,* **16,** 406–425.

——, ——, and H. Su, 2001: Ocean-atmosphere-land feedbacks in an idealized monsoon. *Quart. J. Roy. Meteor. Soc.,* **127,** 1869–1892.

Clement, A. C., A. Hall, and A. J. Broccoli, 2004: The importance of precessional signals in the tropical climate. *Climate Dyn.,* **22,** 327–341.

Couhert, A., T. Schneider, J. Li, D. E. Waliser, and A. M. Tompkins, 2010: The maintenance of the relative humidity of the subtropical free troposphere. *J. Climate,* **23,** 390–403.

Dirmeyer, P. A., 1998: Land-sea geometry and its effect on monsoon circulations. *J. Geophys. Res.,* **103** (D10), 11 555–11 572.

Emanuel, K. A., 1994: *Atmospheric Convection.* Oxford University Press, 580 pp.

——, 1995: On thermally direct circulations in moist atmospheres. *J. Atmos. Sci.,* **52,** 1529–1534.

Gadgil, S., 2003: The Indian monsoon and its variability. *Annu. Rev. Earth Planet. Sci.,* **31,** 429–467.

Held, I. M., 2001a: The general circulation of the atmosphere. *Proc. 2000 Program in Geophysical Fluid Dynamics,* Woods Hole Oceanographic Institution Tech. Rep. WHOI-2001-03, R. Salmon, Ed., Woods Hole Oceanographic Institution, 198 pp. [Available online at http://hdl.handle.net/1912/15.]

——, 2001b: The partitioning of the poleward energy transport between the tropical ocean and atmosphere. *J. Atmos. Sci.,* **58,** 943–948.

——, and A. Y. Hou, 1980: Nonlinear axially symmetric circulations in a nearly inviscid atmosphere. *J. Atmos. Sci.,* **37,** 515–533.

Hsu, Y.-H., C. Chou, and K.-Y. Wei, 2010: Land–ocean asymmetry of tropical precipitation changes in the mid-Holocene. *J. Climate,* **23,** 4133–4151.

Jackson, C. S., and A. J. Broccoli, 2003: Orbital forcing of Arctic climate: Mechanisms of climate response and implications for continental glaciation. *Climate Dyn.,* **21,** 539–557.

Joussaume, S., and P. Braconnot, 1997: Sensitivity of paleoclimate simulation results to season definitions. *J. Geophys. Res.,* **102** (D2), 1943–1956.

Kang, S. M., and I. M. Held, 2012: Tropical precipitation, SSTs and the surface energy budget: A zonally symmetric perspective. *Climate Dyn.,* **38,** 1917–1924, doi:10.1007/s00382-011-1048-7.

Klinger, B. A., and J. Marotzke, 2000: Meridional heat transport by the subtropical cell. *J. Phys. Oceanogr.,* **30,** 696–705.

Kutzbach, J. E., 1981: Monsoon climate of the early Holocene: Climate experiment with the Earth's orbital parameters for 9000 years ago. *Science,* **214,** 59–61.

——, and Z. Liu, 1997: Response of the African monsoon to orbital forcing and ocean feedbacks in the middle Holocene. *Science,* **278,** 440–443.

Legrande, A. N., and G. A. Schmidt, 2009: Sources of Holocene variability of oxygen isotopes in paleoclimate archives. *Climate Past,* **5,** 441–455.

Lindzen, R. S., and S. Nigam, 1987: On the role of sea surface temperature gradients in forcing low-level winds and convergence in the tropics. *J. Atmos. Sci.,* **44,** 2418–2436.

——, and A. Y. Hou, 1988: Hadley circulations for zonally averaged heating centered off the equator. *J. Atmos. Sci.,* **45,** 2416–2427.

Merlis, T. M., and T. Schneider, 2011: Changes in zonal surface temperature gradients and Walker circulations in a wide range of climates. *J. Climate,* **24,** 4757–4768.

——, ——, S. Bordoni, and I. Eisenman, 2013a: Hadley circulation response to orbital precession. Part I: Aquaplanets. *J. Climate,* **26,** 740–753.

——, ——, ——, and ——, 2013b: The tropical precipitation response to orbital precession. *J. Climate,* in press.

Neelin, J. D., 2007: Moist dynamics of tropical convection zones in monsoons, teleconnections, and global warming. *The Global Circulation of the Atmosphere,* T. Schneider and A. H. Sobel, Eds., Princeton University Press, 267–301.

Nie, J., W. R. Boos, and Z. Kuang, 2010: Observational evaluation of a convective quasi-equilibrium view of monsoons. *J. Climate,* **23,** 4416–4428.

O'Gorman, P. A., 2011: The effective static stability experienced by eddies in a moist atmosphere. *J. Atmos. Sci.,* **68,** 75–90.

——, and T. Schneider, 2008: Energy of midlatitude transient eddies in idealized simulations of changed climates. *J. Climate,* **21,** 5797–5806.

Peters, M. E., Z. Kuang, and C. C. Walker, 2008: Analysis of atmospheric energy transport in ERA-40 and implications for simple models of the mean tropical circulation. *J. Climate,* **21,** 5229–5241.

Phillipps, P. J., and I. M. Held, 1994: The response to orbital perturbations in an atmospheric model coupled to a slab ocean. *J. Climate,* **7,** 767–782.

Pierrehumbert, R. T., 2010: *Principles of Planetary Climate.* Cambridge University Press, 688 pp.

Plumb, R. A., and A. Y. Hou, 1992: The response of a zonally symmetric atmosphere to subtropical thermal forcing: Threshold behavior. *J. Atmos. Sci.,* **49,** 1790–1799.

Privé, N. C., and R. A. Plumb, 2007: Monsoon dynamics with interactive forcing. Part I: Axisymmetric studies. *J. Atmos. Sci.,* **64,** 1417–1430.

Schneider, T., 2006: The general circulation of the atmosphere. *Annu. Rev. Earth Planet. Sci.,* **34,** 655–688.

——, and S. Bordoni, 2008: Eddy-mediated regime transitions in the seasonal cycle of a Hadley circulation and implications for monsoon dynamics. *J. Atmos. Sci.,* **65,** 915–934.

——, and C. C. Walker, 2008: Scaling laws and regime transitions of macroturbulence in dry atmospheres. *J. Atmos. Sci.,* **65,** 2153–2173.

——, K. L. Smith, P. A. O'Gorman, and C. C. Walker, 2006: A climatology of tropospheric zonal-mean water vapor fields and fluxes in isentropic coordinates. *J. Climate,* **19,** 5918–5933.

——, P. A. O'Gorman, and X. J. Levine, 2010: Water vapor and the dynamics of climate changes. *Rev. Geophys.,* **48,** RG3001, doi:10.1029/2009RG000302.

Sobel, A. H., and T. Schneider, 2009: Single-layer axisymmetric model for a Hadley circulation with parameterized eddy momentum forcing. *J. Adv. Model. Earth Syst.,* **1,** 10, doi:10.3894/JAMES.2009.1.10.

Su, H., and J. D. Neelin, 2005: Dynamical mechanisms for African monsoon changes during the mid-Holocene. *J. Geophys. Res.,* **110,** D19105, doi:10.1029/2005JD005806.

Walker, C. C., and T. Schneider, 2006: Eddy influences on Hadley circulations: Simulations with an idealized GCM. *J. Atmos. Sci.,* **63,** 3333–3350.